Effects of Temperature on Rhodopsin Photointermediates from Lumirhodopsin to Metarhodopsin II†

Thorgeir E. Thorgeirsson, James W. Lewis, Stacie E. Wallace-Williams, and David S. Kliger*

Department of Chemistry and Biochemistry, University of California at Santa Cruz, Santa Cruz, California 95064

Received July 29, 1993; Revised Manuscript Received September 16, 1993•

ABSTRACT: Absorbance changes following the photolysis of mildly sonicated membrane suspensions of bovine rhodopsin are monitored using multichannel detection at 15, 20, 25, 30, and 35 °C. Difference spectra collected with microsecond time resolution are analyzed by singular value decomposition and multiexponential fitting. Several kinetic schemes are tested using methods that compare the observed rates and associated spectral amplitudes to the eigenvalues and eigenvectors of kinetic matrices. The time evolution of the spectra is more complex than can be accounted for by the traditional lumi → metarhodopsin I ⇄ metarhodopsin II scheme. Above 25 °C, the formation of metarhodopsin II is achieved without a large transient accumulation of metarhodopsin I. Within the framework of first-order kinetics, the observations are explained by simple kinetic schemes that lead to the formation of a deprotonated Schiff's base species temporally distinct from metarhodopsin II directly upon the decay of lumirhodopsin.

Rhodopsin (rho)[1] is the light-absorbing pigment of retinal rod photoreceptor cells. Rhodopsin contains an intrinsic chromophore, 11-*cis*-retinal, that is covalently bound to the protein (opsin) moiety via a protonated Schiff's base linkage to a lysine residue. Upon absorption of a photon, the rhodopsin molecule becomes active and binds to its G-protein, transducin. This interaction initiates an enzyme cascade resulting in the closure of sodium channels in the rod membrane, leading to synaptic transmission (Stryer, 1986).

The first step in vision is a photoisomerization around the 11,12 double bond of the chromophore, yielding an all-transoid configuration, an event that occurs within 200 fs (Schoenlein *et al.*, 1991). Following this, a series of thermal reactions occurs within the rhodopsin molecule leading to the formation of meta II, the photointermediate which activates transducin. The existence of intermediate processes was first shown by low-temperature trapping techniques, which yielded the traditional scheme illustrated in Scheme I (Yoshizawa, 1972; Matthews *et al.*, 1963). In Scheme I, the numbers above the arrows are the transition temperatures below which the preceding intermediate is stable, and the wavelengths indicate the spectral maxima of the trapped intermediates.

Recent spectroscopic studies at ambient temperatures have characterized new photointermediates, leading to some refinements in the above scheme [reviewed by Lewis and Kliger (1992)]. Much progress has been made regarding the earlier steps of the transformations leading to the formation of lumi, but there is less agreement regarding later events.

meta II (λ_{max} = 380 nm) contains a deprotonated retinal Schiff's base chromophore and exists in equilibrium with meta I (λ_{max} = 477 nm), which contains a protonated chromophore. Matthews *et al.* (1963) demonstrated that meta II is an intermediate distinct from *all-trans*-retinal and showed that

Scheme I

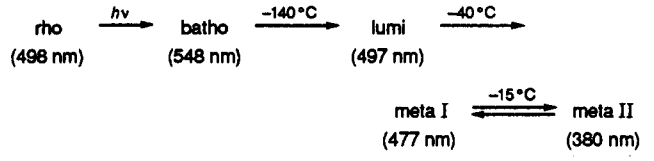

low pH's and high temperatures favor the meta II form of the pigment. Matthews *et al.* (1963) calculated 13.1 kcal/mol and 46.5 eu for the enthalpy and entropy of activation, respectively, in digitonin suspensions. At physiological temperatures, the meta II form is thus strongly favored. The meta I ⇄ meta II equilibrium is established in milliseconds at 37 °C. Upon photolysis at temperatures below −15 °C only meta I is formed, and it converts to meta II as the temperature is raised. This is generally considered to mean that meta I is the precursor to meta II. Kinetic measurements at elevated temperatures, however, have repeatedly shown the scheme to be more complex than the one described above (Lewis & Kliger, 1992).

Almost all studies of the meta I ⇄ meta II transition to date involve single-wavelength measurements at one or a few wavelengths. As lumi is formed in less than 1 μs, measurements of its decay with an adequate signal-to-noise ratio using a continuous probe source require probe intensities that potentially cause significant bleaching on the time scale of meta II formation. Thus, the kinetics of the lumi → meta I and meta I → meta II reactions are often studied separately. As the photointermediates have overlapping spectra, this approach is only valid at lower temperatures where the decay of lumi and the formation of meta II are well separated in time. For reviews of the results from such measurements, see Ostroy (1977), Hofmann (1986), and Lewis and Kliger (1992).

The difficulties in the interpretation of results from single-wavelength measurements at ambient temperatures arise from the spectral overlap and poorly separated decay times of the late photointermediates. Although conclusions depend on whether the contribution to absorbance at single wavelengths is estimated from low-temperature spectra (Applebury *et al.*, 1974; Parkes & Liebman, 1984) or is allowed to vary with

† Supported by Grant EY00983 from the National Institutes of Health.
* Address correspondence to this author.
• Abstract published in *Advance ACS Abstracts,* December 1, 1993.
[1] Abbreviations: batho, bathorhodopsin; DTT, dithiothreitol; EDTA, ethylenediaminetetraacetic acid; lumi, lumirhodopsin; meta, metarhodopsin; OMA, optical multichannel analyzer; PIPES, piperazine-*N*,*N*′-bis(2-ethanesulfonic acid); rho, rhodopsin; Tris, tris(hydroxymethyl)aminomethane.

0006-2960/93/0432-13861$04.00/0

temperature (Straume *et al.*, 1990), it is clear that the formation rate of meta II approaches the rate of lumi decay near physiological temperatures (Applebury *et al.*, 1974; Lewis *et al.*, 1981; Straume *et al.*, 1990). We recently measured the absorption changes following photolysis of rhodopsin in membrane suspensions with microsecond resolution using multichannel detection (Thorgeirsson *et al.*, 1992). Analysis of the spectra using SVD and global exponential fitting suggested that the decay of lumi results in the formation of a species with an absorption spectrum similar to that of meta II at short delays following photolysis, much earlier than could be accounted for by Scheme I.

Here we extend our studies to include the effects of temperature on the decay of lumi and the formation of other intermediates leading to meta II. Photolysis-induced absorbance changes [$A(\lambda,t)$ (with laser excitation) – $A(\lambda)$ (without laser excitation)] are monitored at five temperatures (15, 20, 25, 30, and 35 °C) with microsecond time resolution using a pulsed probe source and multichannel detection. The aim of the study is to find the simplest kinetic scheme that can explain the optical changes using a single set of temperature-invariant spectra for the photointermediates.

MATERIALS AND METHODS

Sample Preparation. Hypotonically washed membrane suspensions of rhodopsin were prepared and sonicated as described previously (Thorgeirsson *et al.*, 1992). For each photolysis experiment, the sample consisted of about 70 mL of 0.25 mg of rho/mL of low salt (2 mM $MgCl_2$, 0.1 mM EDTA) 10 mM Tris or PIPES buffer at pH 7.0.

Photolysis Experiments. Photolysis experiments were performed using an apparatus described previously (Lewis *et al.*, 1987a; Hug *et al.*, 1990). Rhodopsin was photolyzed using vertically polarized 477-nm light (7 ns FWHM, 0.7 mJ/pulse/10 mm^2 area) from a dye laser pumped by the third harmonic of a Nd:YAG laser. The probe source was an EG&G FXQ-856 xenon flash lamp (5 μs duration), and light intensities were measured using an intensified optical multichannel analyzer (OMA) system equipped with a photographic filter (Lewis *et al.*, 1987b). Constant sample temperature (±0.2 °C) was maintained using a copper insert connected to a water bath.

Samples were held on ice until loaded into the syringe pump which delivered them to the cell after each laser pulse. Prior to loading the syringe, an aliquot of sample was warmed to room temperature and degassed under vacuum to prevent dissolved gasses from coming out of solution to form bubbles in the cell. Only immediately prior to photolysis (<1 min) was the sample actually exposed to the temperature prevailing in the cell.

Transient difference spectra were calculated by taking the log of the ratio of the probe intensities without and with sample photolysis for both horizontal ($\perp$) and vertical ($\parallel$) polarizations of the probe beam. Average optical density, free from artifacts due to molecular rotation, was then calculated using

$$\Delta OD = (\Delta OD_{\parallel} + 2\Delta OD_{\perp})/3 \quad (1)$$

The data from the OMA consist of ΔOD values at 720 different wavelengths between 320 and 720 nm. The number of data points was reduced to about 200 by box averaging over each set of three consecutive channels and by deleting ΔOD values for wavelengths longer than 700 nm and shorter than 350 nm (where low probe intensities resulted in excessive noise). The difference spectra were then transferred to a Sun workstation for analysis.

In preparation for analysis, kinetic data from experiments at the same temperature (n = 3 or 4) were first scaled by minimizing:

$$\Delta OD_i - k_j \Delta OD_j \quad (2)$$

where ΔOD_i is a matrix of ΔOD values from an experiment used as reference, and ΔOD_j are matrices containing the results from other measurements. Values of k_j were between 0.9 and 1.1 and were in excellent agreement with scaling factors obtained from measurements of the amount of rho photolyzed in Ammonyx LO detergent, as described by Albeck *et al.* (1989).

Data were analyzed using routines from the Matlab software package (The Math Works) combining singular value decomposition (SVD) and global exponential fitting (Hug *et al.*, 1990; Thorgeirsson *et al.*, 1991). Orthonormal basis spectra obtained from SVD are used to represent the entire data matrix in a nonlinear least-squares (Nelder–Meade simplex) fit to a sum of exponentials:

$$\Delta OD(\lambda,t) = \sum_{i=0}^{N} \mathbf{b}_i(\lambda) e^{-k_i t} \quad (3)$$

where N is the number of exponentials, k_i are the observed rate constants, and $\mathbf{b}_i(\lambda)$ are the b spectra that are associated with the apparent rates. The fitting procedure minimizes the square of the difference between the data and the fit. The application of SVD removes noise and reduces computational time (Henry & Hofrichter, 1992; Thorgeirsson *et al.*, 1992).

Singular Value Decomposition. The SVD analysis can give an estimate of how many spectrally distinct intermediates are needed to reproduce the data within the noise of the experiment. Each difference spectrum can be expressed in terms of the concentrations (c_i) and spectra (ϵ_i) of the intermediates and a constant spectrum (BLEACH). For the traditional scheme (1 cm path length), this would correspond to

$$\Delta OD(\lambda,t) = c_{\text{lumi}}\epsilon_{\text{lumi}} + c_{\text{meta I}}\epsilon_{\text{meta I}} + c_{\text{meta II}}\epsilon_{\text{meta II}} - \text{BLEACH} \quad (4)$$

The spectrum at 1 μs will be

$$\Delta OD(\lambda, 1\ \mu s) = C_0\epsilon_{\text{lumi}} - \text{BLEACH} \quad (5)$$

if lumi is the only thermally decaying photointermediate present at 1 μs and C_0 is the amount of rhodopsin photolyzed. The concentrations of lumi, meta I, and meta II must always add up to C_0. The contribution from the constant term can be removed by subtracting the spectrum at 1 μs from all of the difference spectra:

$$\Delta OD(\lambda,t) - \Delta OD(\lambda, 1\ \mu s) = c(t)_{\text{meta I}}\{\epsilon_{\text{meta I}} - \epsilon_{\text{lumi}}\} + c(t)_{\text{meta II}}\{\epsilon_{\text{meta II}} - \epsilon_{\text{lumi}}\} \quad (6)$$

This allows a convenient check of the number of spectrally distinct intermediates through the use of SVD. First the difference spectrum at 1 μs is subtracted from all of the difference spectra, and the resulting data matrix of double difference spectra is decomposed into basis spectra. The basis spectra obtained in this way will not necessarily be the difference spectra between the intermediates as in eq 6, but in the case of three spectrally distinct intermediates, the effective rank (Henry & Hofrichter, 1992) of the matrix of double difference spectra will equal 2.

The differential equations describing the rate of decay for each intermediate in matrix form are (master equation)

$$\dot{\mathbf{c}}(t) = \mathbf{K}\mathbf{c}(t) \tag{7}$$

where $\mathbf{c}(t)$ is the column vector of the concentrations of intermediates and $\dot{\mathbf{c}}(t)$ the corresponding time derivatives. $\mathbf{K}$ is the kinetic matrix constructed from the microscopic rate constants, such that (for a scheme of n intermediates)

$$\mathbf{K} = \begin{bmatrix} -\sum_i k_{1,i} & \cdots & k_{j,1} & \cdots & k_{n,1} \\ \vdots & \ddots & \vdots & \iddots & \vdots \\ k_{1,j} & \cdots & -\sum_i k_{j,i} & \cdots & k_{n,j} \\ \vdots & \iddots & \vdots & \ddots & \vdots \\ k_{1,n} & \cdots & k_{j,n} & \cdots & -\sum_i k_{n,i} \end{bmatrix} \tag{8}$$

where $k_{i,j}$ denotes the rate constant for the transition from intermediate i to intermediate j. The solution can be expressed in terms of the eigenvectors ($\mathbf{a}_i$) and eigenvalues (α_i) of the kinetic matrix. That is,

$$\mathbf{c}(t) = \sum_{i=1}^{n} f_i \mathbf{a}_i e^{\alpha_i t} \tag{9}$$

where the constants, f_i, can be determined from the elements of $\mathbf{c}(0)$ (Millhauser & Oswald, 1988).

Thus, the apparent rates obtained from an exponential fit correspond to the eigenvalues of the kinetic matrix, and the b spectra are related to the eigenvectors through

$$\mathbf{b}_i(\lambda) = f_i \mathbf{a}_i(\lambda)\epsilon(\lambda) \tag{10}$$

where $\mathbf{a}_i$ is a $(1 \times n)$ eigenvector and the columns of $\epsilon(\lambda)$ contain the spectra of the intermediates. The spectra in $\epsilon(\lambda)$ can be the true spectra of intermediates or $\epsilon_i(\lambda)$ –BLEACH spectra, as here when difference spectra are measured. For certain simple kinetic schemes, these relationships allow the calculation of intermediate spectra directly from the output of the exponential fitting process (Thorgeirsson *et al.*, 1992). Also, when the spectra of the intermediates are known, microscopic rate constants can be found by optimization, varying the elements of the kinetic matrix to obtain a fit to both the observed b spectra and the measured apparent rates.

RESULTS

Figure 1 shows absorption difference spectra measured at 15, 25, and 35 °C. Qualitatively, these spectra are consistent with the traditional scheme. At late times following photolysis, the difference spectra show the presence of meta I and meta II, and at early times lumi. During the formation of meta I (λ_{max} = 477 nm) from lumi (λ_{max} = 497 nm), absorbance is expected to rise transiently near 480 nm. This is the case at 15 °C, but at higher temperatures the spectra show a continuous decrease with time in that region. This observation is, in itself, not necessarily inconsistent with the simple scheme lumi → meta I ⇄ meta II, as it could merely indicate that meta I does not build up. The results from global exponential fitting, however, show that the explanation is not that simple.

Singular Value Decomposition. SVD is mainly used to reduce computational time. When a large enough number of basis spectra is used, the truncated representation is equivalent to the entire data set within experimental noise. SVD analysis of individual data sets showed that the effective rank was close to 3 at all temperatures. For the global analysis, we used the first four basis spectra and checked that using a larger number did not lead to changes in observed lifetimes. In addition to reducing computational time, the output from SVD provides an estimate of the number of spectrally distinct intermediates. We performed the analysis described in Materials and Methods (eqs 4–6) and found that, at each temperature, almost all of the spectral information is indeed contained in the first two basis spectra. The first basis spectrum resembled the meta II – lumi difference spectrum, and the second basis spectrum resembled the meta I – lumi difference spectrum. The importance of the second basis spectrum decreased with increasing temperature. This is reflected in the singular values (eigenvalues of the matrix S), which were as follows (as percentages of largest singular value): 100, 12.7, 5.2, 3.3, 1.5, ..., 0.7 (15 °C); 100, 4.6, 3.4, 0.8, 0.6, ..., 0.4 (25 °C); 100, 2.0, 1.4, 0.9, 0.5, ..., 0.3 (35 °C).

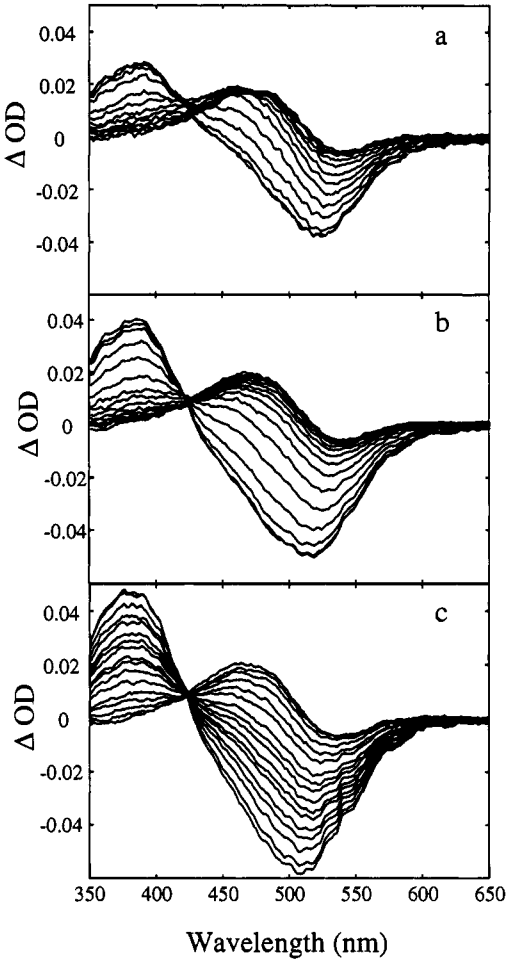

FIGURE 1: Transient difference spectra obtained for sonicated disk suspensions after excitation at 477 nm with a 7-ns laser pulse (fluence ≈ 5 mJ/cm²). (a) At 15 °C. Times following excitation: 1, 6, 12, 25, 50, 100, 200, 400, and 800 μs and 1.5, 3, 6, 12, 24, 50, 100, 200, and 400 ms. (b) At 25 °C. Times following excitation: 1, 3, 6, 12, 25, 50, 100, 200, 400, and 800 μs and 1.5, 3, 6, 12, 24, 50, and 75 ms. (c) At 35 °C. Times following excitation: 1, 6, 12, 25, 50, 100, 200, 300, 400, 600, and 800 μs and 1.5, 3, 6, and 12 ms.

Exponential Fitting. Figure 2 shows the b spectra from global fits to the data sets of Figure 1. The lifetimes at all temperatures are shown in Table I. Figure 3 shows Arrhenius plots for the apparent rate constants. At 15 °C the results from exponential fitting are consistent with the traditional scheme. Only two exponentials are required to fit the data within experimental error, and the spectral changes are consistent with the formation of metal I from lumi followed by a net meta I → meta II transition. At 20 °C and above,

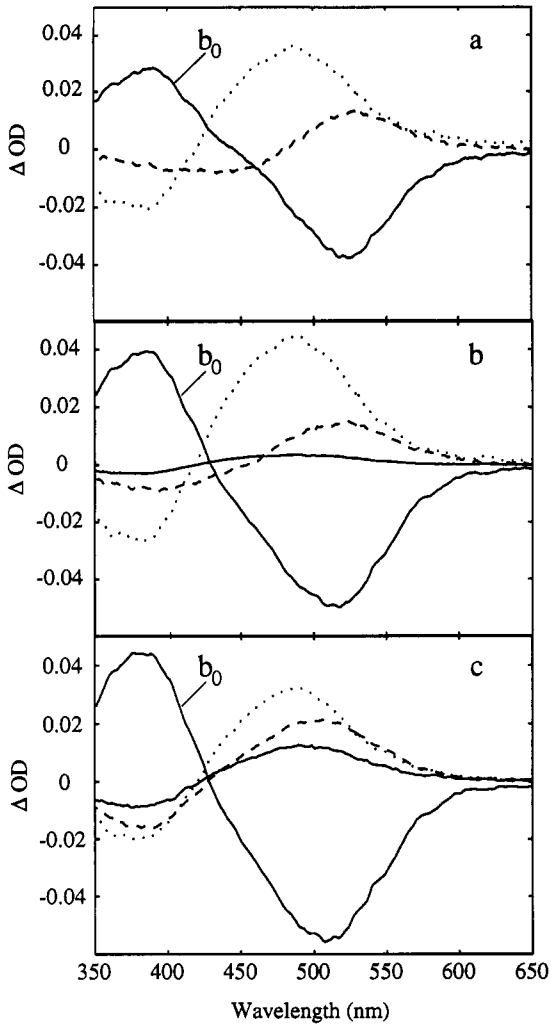

FIGURE 2: Absorbance changes (b spectra) associated with the apparent rates from exponential fits of data sets obtained at 15, 25, and 35 °C. (a) b spetra obtained from experiments at 15 °C. A two-exponential fit was sufficient to fit the data within experimental error. (b) b spectra obtained from experiments at 25 °C (c) b spectra obtained from experiments at 35 °C. The time-independent b spectrum at each temperature is labeled b_0. The line types for the time-dependent b spectra are as follows: (—) b_1, the b spectra associated with the fastest component; (- - -) b_2; (···) b_3, the spectral changes associated with the slowest component. Refer to Table I for the observed lifetimes.

Table I

	15 °C	20 °C	25 °C	30 °C	35 °C
			Two-Exponential Fits		
τ_1 (ms)	2.8 ± 0.1	1.8 ± 0.2	0.89 ± 0.1	0.225 ± 0.05	0.086 ± 0.02
τ_2 (ms)	43 ± 1	21.9 ± 0.2	9.7 ± 0.9	3.8 ± 0.4	1.6 ± 0.1
SSR[a]	2.4	3.3	3.7	4.1	4.5
			Three-Exponential Fits		
τ_1 (μs)		160 ± 80	89 ± 30	55 ± 20	39 ± 15
τ_2 (ms)	2.8 ± 0.1	2.07 ± 0.2	1.58 ± 0.2	0.76 ± 0.15	0.46 ± 0.05
τ_3 (ms)	43 ± 1	21.2 ± 0.2	10.2 ± 0.6	4.5 ± 0.1	2.38 ± 0.05
SSR[a]		2.7	2.0	2.5	2.0

[a] The total sum of squared residuals is normalized to a noise estimate, i.e., the value expected for a perfect fit. The uncertainties in the apparent rate constants were estimated from the distribution of observed rates obtained from analysis of individual experiments (Thorgeirsson *et al.*, 1992; Thorgeirsson, 1992).

three exponentials are required to fit the data within the noise. The amplitude of the fastest component is small at 20 and 25 °C but increases with temperature, such that at 35 °C it accounts for about 20% of the total rise in absorbance near 380 nm.

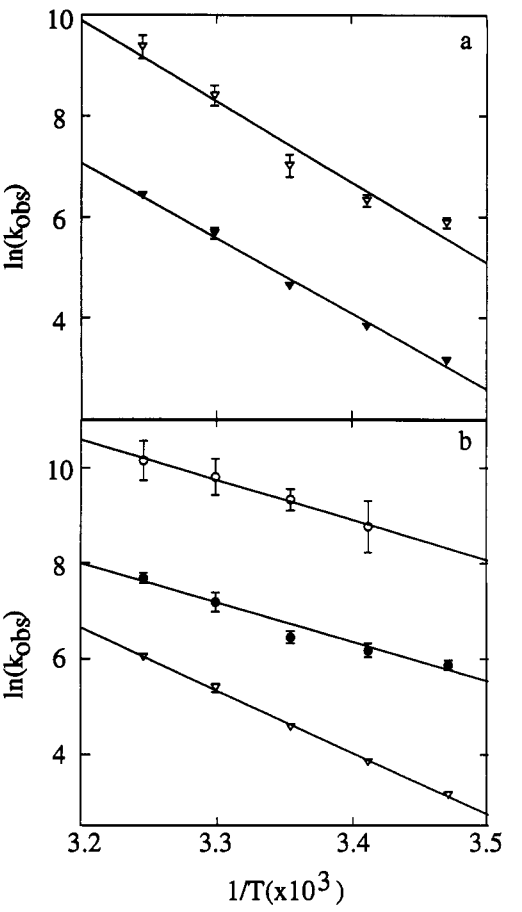

FIGURE 3: Arrhenius plots for the observed rate constants. (a) Plot of $\ln(k_{obs})$ vs $(1/T)$ with apparent rate constants from the two-exponential fits: (▼) k_1; (▽) k_2. (b) Plot of $\ln(k_{obs})$ vs $(1/T)$ using apparent rate constants from the three-exponential fits: (○) k_1; (●) k_2; (▽) k_3. Estimated uncertainties are indicated by error bars when the error exceeds the size of the graphic symbol. Activation energies are (kcal) as follows: two-exponential fits, 31.8 (k_1) and 29.4 (k_2); three-exponential fits, 16.7 (k_1), 16.3 (k_2), and 26.0 (k_3).

To account for three exponentials within the framework of first-order kinetics, it is necessary to postulate a kinetic scheme containing four intermediates (Nagle *et al.*, 1982). The results from the SVD analysis indicate that the spectrum for this additional intermediate can be expressed as a linear combination of the spectra for lumi, meta I, and meta II. Explanation of the data with kinetic schemes involving only three intermediates (i.e., lumi, meta I, and meta II) would require that at least some of the kinetic rate constants change with time or that at least one of the transitions has a distribution of kinetic barriers.

The traditional mechanism should not be discarded on this basis alone, however, since two exponentials fit the data to a first approximation. More importantly, the spectral changes associated with the observed rates in the *two-exponential* fits at the higher temperatures are not consistent with the traditional scheme. We have previously discussed how the data deviate from what is expected on the basis of the traditional scheme at 25 °C (Thorgeirsson *et al.*, 1992). Figure 4 illustrates this further. When intermediate spectra are calculated assuming the traditional scheme, the meta I spectrum varies with temperature. Were the traditional scheme valid, all of the intermediates would have spectra that are relatively independent of temperature. The fact that they do not implies that this temperature-dependent component arises from more than one intermediate. The simple scheme, lumi → meta I ⇄ meta II, therefore cannot account for our

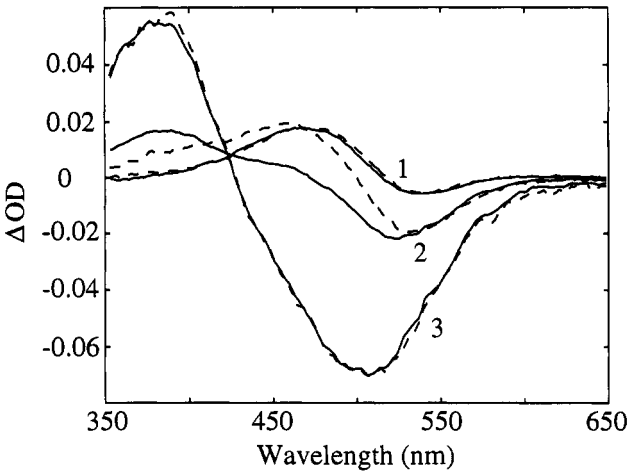

FIGURE 4: Intermediate–BLEACH spectra of intermediates at 15 and 35 °C. (– –) Intermediate–BLEACH spectra calculated from the *b* spectra obtained at 15 °C, assuming the simple scheme lumi → meta I ⇄ meta II. The equilibrium constant ($K = 0.75$) for the meta I ⇄ meta II equilibrium was chosen such that the amplitude of the spectrum for meta II – BLEACH at 500 nm was equal to that of the spectrum of the sample following photolysis in Ammonyx LO detergent. (—) Intermediate–BLEACH spectra calculated from the *b* spectra from the two-exponential fit to data at 35 °C assuming the simple scheme lumi → meta I ⇄ meta II. The meta I – BLEACH spectrum differs from that calculated using data obtained at 15 °C. The pairs of curves correspond to the lumi – BLEACH (1), meta I – BLEACH (2), and meta II – BLEACH (3) spectra. Application of Scheme I to the data thus yields a temperature-dependent meta I – BLEACH spectrum (2).

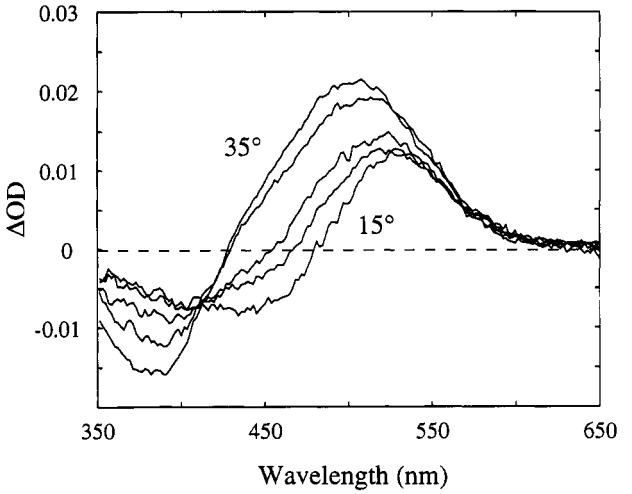

FIGURE 5: Spectral changes (*b* spectra) associated with the second apparent rate (τ_2) from exponential fits at all temperatures. The spectral changes associated with τ_2 show a crossing point near 415 nm that is offset from zero. This crossing point is near the isosbestic point between meta I_{480} and meta II, and the changes are consistent with the transition of lumi into a mixture of meta I and a species absorbing maximally near 380 nm.

results at the higher temperatures, and our previous conclusion that the decay of lumi results in the nearly simultaneous formation of meta I and a species absorbing near 380 nm is supported by the current results. Since this intermediate appears at a similar time following photolysis as meta I, we will refer to this new intermediate from this point on as meta I_{380} and the traditional meta I intermediate as meta I_{480}.

Possible Kinetic Schemes. We previously suggested the scheme (Scheme II) with a fast (100 μs) metal I_{380} ⇄ meta I_{480} equilibrium step to explain the results at 25 °C. We

Scheme II

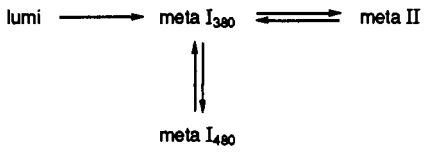

tested this scheme using the methods outlined previously (Thorgeirsson *et al.*, 1992) with data from all five temperatures. The amplitude of the fast component becomes larger than that predicted by this scheme at the higher temperatures. The deviation was found to be within experimental error at 30 °C. At 35 °C, however, the amplitude of the fast component is approximately 3 times what Scheme II predicts.

There are many possible extensions of Scheme I, and rigorously testing all of them is impossible. The kinetic schemes that we considered are listed in the Appendix. Several general conclusions regarding the underlying kinetic scheme can be drawn from visual inspection of the results from the exponential fitting process to aid in selecting candidate mechanisms.

Temperature-Dependent Spectrum of the Second Component. When Scheme I is used to calculate intermediate spectra, a temperature-dependent meta I spectrum is obtained (Figure 4). Figure 5 shows the changes occurring in the second component *b* spectra (of the three exponential fits) with temperature. The *b* spectra associated with the second component (τ_2) all cross near 415 nm. While this crossing point is near the meta I–meta II isosbestic point it is negatively offset from zero. The second *b* spectrum therefore cannot represent a simple transition between two species. Rather, the changes are consistent with a transition from lumi to a mixture of meta I and a species with a spectrum similar to that of meta II, where the amount of the meta II-like species is increasing with temperature. The crossing point is negatively offset because lumirhodopsin has lower extinction near 415 nm than both meta I and meta II (or meta I_{380}). The Arrhenius plot for the second apparent rate constant shows deviations from linearity (Figure 3). It appears that the second rate constant increases faster with temperatures above 25 °C than below. This suggests that the second apparent rate constant is composed of at least two microscopic rate constants. This in turn suggests kinetic schemes involving either branching at the lumi intermediate or a back-reaction to lumi that becomes important at higher temperatures.

Temperature-Invariant lumi Spectrum. Figure 6 shows the difference spectra at the earliest time (1 μs) following photolysis at all the temperatures. These spectra are all identical within experimental error. This suggests that the appearance of the fast process is not due to branching before the decay of the lumi intermediate. The formation of lumi is biexponential, but these processes have been shown to be consistent with the formation of a single lumi intermediate from batho in a two-step process (Hug *et al.*, 1990). Thus, it is likely that the spectrum at 1 μs represents a single intermediate.

Results from 15 °C Yield Intermediate Spectra. The results from 15 °C are consistent with the traditional scheme (Scheme I). Therefore, the intermediate–BLEACH spectra calculated using the *b* spectra obtained from the two-exponential fit at 15 °C are most likely very good first approximations of the spectra for lumi, meta I_{480}, and meta II (Figure 4).

Parallel Schemes. The observations outlined above exclude a set of parallel schemes. Take, for example, Scheme III, where meta I'_{480} is formed in parallel with lumi, such that it is already present at 1 μs. If meta I'_{480} decays rapidly to form meta II′ and the fraction of meta I'_{480} increases with temperature, this scheme would account for the appearance

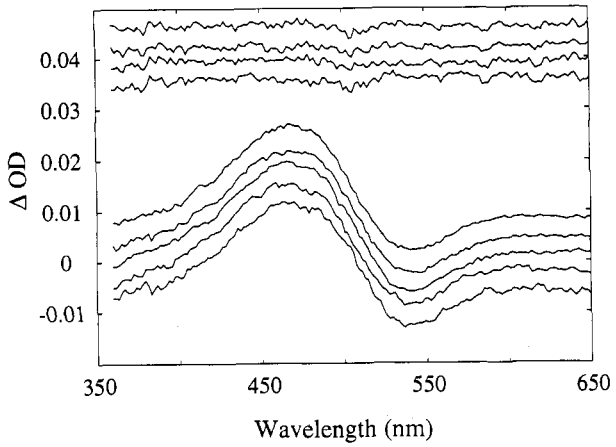

FIGURE 6: Difference spectra at 1 μs following laser excitation. The spectra (bottom) are offset by 5 mOD for ease of comparison. The temperatures at which the spectra were measured are (from bottom to top) 15, 20, 25, 30, and 35 °C. At the top of the figure, the double difference spectra obtained by subtracting the 1-μs spectrum at 15 °C from spectra at the other temperatures are shown. The spectra at 1 μs are all identical within experimental error, suggesting that branching does not occur before the decay of lumirhodopsin.

Scheme III

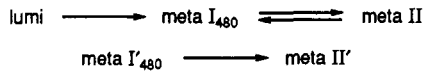

of the fast component at temperatures above 20 °C. This scheme, on the other hand, predicts changes in the initial spectrum (at 1 μs), and that the spectral changes associated with the second component would resemble the meta I – lumi difference spectrum at all temperatures. The temperature invariance of the spectrum at 1 μs and the observed changes in the spectral changes associated with the second lifetime thus allow the rejection of Scheme III.

Branched Schemes. Since Scheme II failed to explain the large amplitude of the fastest process at 35 °C, we looked for alternative explanations for the fast component. Scheme II assigned the fast process to the meta $I_{380} \rightleftarrows$ meta I_{480} step, but a fast component of a similar shape could be due to a rapid equilibrium between lumi and meta I_{380}. We thus decided to test Scheme IV.

Scheme IV

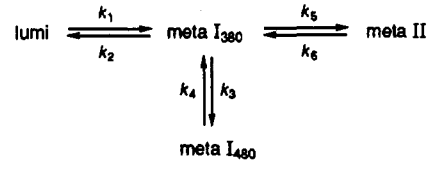

The methods we have developed to calculate intermediate spectra for any first-order kinetic scheme require a numeric kinetic matrix, and become somewhat cumbersome when the kinetic matrix is underdetermined. In our previous study, we simply guessed two microscopic rate constants (i.e., by guessing two equilibrium constants) and calculated intermediate spectra for each guess (Thorgeirsson *et al.*, 1992). In principle, Scheme IV could thus be tested by setting up equations relating the eigenvalues of the kinetic matrix and the observed rate constants and guessing three, thereby obtaining a numeric kinetic matrix. Testing Scheme IV took a different approach using the spectra calculated for the photointermediates from results obtained at 15 °C.

In this analysis, we used the spectra obtained from the global analysis at 15 °C (Figure 4) as an initial guess to calculate

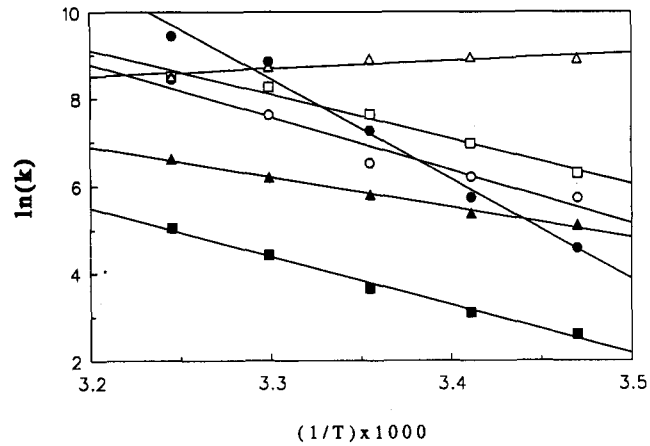

FIGURE 7: Arrhenius plots ($\ln(k)$ vs $1/T$) for the microscopic rate constants obtained using Scheme IV: (○) k_1; (●) k_2; (△) k_3; (▲) k_4; (□) k_5; (■) k_6. For the numbering of the microscopic rate constants, see the Results section (Scheme IV).

both *b* spectra and apparent rate constants for this scheme. We then assumed that meta I_{380} has the same spectrum as meta II. By varying the microscopic constants, eigenvalues and eigenvectors for the resulting kinetic matrices were calculated for each choice of microscopic rate constants. At each temperature a simplex routine was used to minimize (1) the squared difference between the measured apparent rate constants and the calculated eigenvalues and (2) the squared difference between the calculated and measured *b* spectra. The resulting microscopic rate constants could then be evaluated by the linearity of their Arrhenius behavior.

The study of Scheme IV is very instructive, as it illustrates the problems associated with interpretating spectral data in terms of schemes involving isospectral intermediates. The combined effect of having two isospectral intermediates and heavily connected equilibria results in multiple solutions to the eigenvalue and eigenvector equations. The fastest process can, for example, arise from any of the three equilibria: (1) from the meta $I_{380} \rightleftarrows$ meta I_{480} step, as was suggested previously (Thorgeirsson *et al.*, 1992); (2) from the lumi $\rightleftarrows$ meta I_{380} step, with the equilibrium favoring lumi at the lower temperatures; and (3) from meta II formation (this occurs when k_5 approaches k_3). The existence of multiple solutions rendered the simplex fitting process ineffective, and the scheme had to be explored by "manually" varying the microscopic rate constants to maintain a linear Arrhenius relationship for all of the microscopic rate constants.

The increase in amplitude of the fastest component at the higher temperatures could not be accounted for by assigning it to the meta $I_{380} \rightleftarrows$ meta I_{480} equilibrium. Assignment to lumi $\rightleftarrows$ meta I_{380} failed at the lower temperatures as the formation rate of meta I_{480} could not be reproduced when the lumi $\rightleftarrows$ meta I_{380} equilibrium strongly favored lumi. The observations could, however, be accounted for at all temperatures by increasing k_5 to values near k_3 at the higher temperatures.

Figure 7 displays the results from this approach as an Arrhenius plot of the microscopic rate constants. The Arrhenius plot shows unusual behavior for k_3, the meta $I_{380} \rightarrow$ meta I_{480} rate constant (Figure 7). It was necessary to allow k_3 to *increase* with decreasing temperature to account for the small amplitude of the fastest component at the lower temperatures. While this behavior is rather strange, Scheme IV cannot be excluded on this basis alone, as the amplitude of the fastest component is small and the fastest lifetime is indeterminate at the lower temperatures.

Figure 7 shows two effects of temperature for Scheme IV: (1) Increasing temperature increases the stability of lumi relative to meta I_{380} and that of meta I_{380} relative to meta I_{480}; (2) high temperature narrows the difference between the formation rates of meta II and meta I_{480}. Thus, at lower temperatures, where $k_3 \gg k_5$, meta II formation occurs via the route lumi → [meta I_{480}, meta I_{380}] → meta II, with a large transient accumulation of meta I. At near-physiological temperatures, on the other hand, meta II is formed to an increase extent via the more direct route lumi ⇄ meta I_{380} ⇄ meta II. This explains the reduced appearance of meta I_{480} at the higher temperatures.

The above suggested that the data might also fit Scheme V. By incorporating a fast lumi ⇄ meta I_{380} equilibrium that

Scheme V

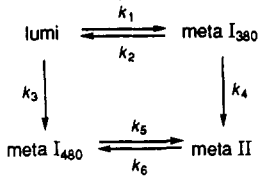

strongly favors lumi at lower temperatures, this scheme can account for the fast component. The apparent rate constant of lumi decay will reflect the lumi → meta I reaction at lower temperatures, with an increasing contribution from the meta I_{380} → meta II reaction as the temperature increases. This would explain the onset of the rapid increase in the second apparent rate constant with temperatures above 25 °C when the fast component becomes significant (Figure 3).

The fitting process outlined above resulted in excellent fits to both the apparent rate constants and the *b* spectra at all temperatures, without any problems with multiple solutions as were encountered for Scheme IV. The initial guess for the spectra for the intermediates was based on the results from the two-exponential fit at 15 °C, and the kinetic matrices obtained in this way were then used to calculate new intermediate spectra from the observed *b* spectra. Using the new intermediate spectra obtained at the higher temperatures (25–35 °C, where the measurements of the fast component were more reliable), the spectra for the photointermediates were generated by averaging the three spectra obtained for each intermediate (lumi, meta I_{380}, meta I_{480}, and meta II) at 25, 30, and 35 °C. The final spectra are displayed in Figure 8. The meta II spectrum is essentially unchanged, but the spectrum for meta I_{480} has a slightly lower extinction near 380 nm and a slightly higher extinction near 480 nm than the spectrum used as the initial guess. The fitting process was then repeated using this new set of spectra. The second iteration resulted in minor changes in the calculated microscopic rate constants. The microscopic rate constants reported here resulted from the second iteration (Table II). The resulting *b* spectra are shown in Figure 9, and Figure 10 shows an Arrhenius plot of the microscopic rate constants. The calculated eigenvalues for the kinetic matrices were equal to the measured apparent rate constants to within one-half the experimental uncertainty for the slowest rate (τ_3) and to within 5% for the two faster rates, where experimental uncertainty was on the order of 10–20%. To evaluate the uncertainties in the microscopic rate constants due to experimental error in the lifetimes from the global fits, the fitting process was repeated for all combinations (8) of the maximum and minimum values for the measured apparent rates. The resulting microscopic rate constants (Table II) all increase

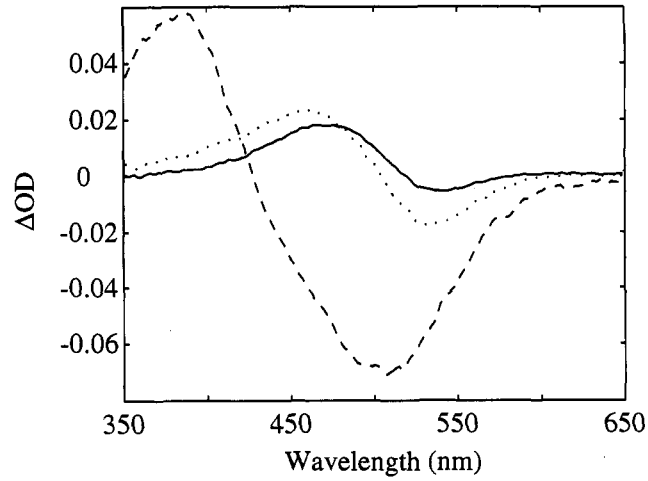

FIGURE 8: Intermediate spectra resulting from the fit to Scheme V. The temperature-invariant spectra were obtained from the analysis outlined in the Results section for Scheme V: (—) lumi – BLEACH; (···) meta I_{480} – BLEACH; (– –) meta I_{380} – BLEACH and meta II – BLEACH. The *b* spectra calculated using the microscopic rate constants displayed in Table II are shown in Figure 9.

with increasing temperature in a linear Arrhenius fashion (Figure 10).

DISCUSSION

We have presented the results of global exponential fitting of data sets containing difference spectra following the photolysis of rhodopsin at five different temperatures. Several general conclusions can be drawn from these results. We conclude that the traditional scheme, lumi → meta I ⇄ meta II, cannot adequately account for our results and that an additional intermediate, meta I_{380}, spectrally similar to meta II but appearing much earlier needs to be added to the scheme.

To proceed further in analyzing our data, we made the following assumptions: (1) the same kinetic scheme applies at all temperatures; (2) spectra of photointermediates are temperature-invariant in the temperature range studied; and (3) lumirhodopsin is the only thermally decaying photointermediate present at 1 μs following the laser pulse. The first two are standard assumptions in work of this nature [see, for example, Nagle *et al.* (1982)]. The third is reasonable given the temperature independence of the spectrum at 1 μs (Figure 6) and results from previous work on the formation of lumi (Hug *et al.*, 1990).

Using these assumptions, we tested several kinetic schemes (see the Appendix) that were likely to account for the observations. The goal was to find the simplest kinetic scheme whose intermediates possess temperature-invariant spectra and whose microscopic rate constants increase with temperature in a linear Arrhenius fashion. A number of schemes were unable to account for our data. These are shown in the Appendix. We were able to fit our data to relatively simple kinetic schemes yielding temperature-invariant spectra.

The Equilibrium Model (Scheme IV). Scheme IV yields linear Arrhenius plots for the microscopic rate constants, although the positive slope of $\ln(k_3)$ vs $1/T$ is unusual. However, this effect could be due to errors in data at the lower temperatures where the rates and amplitudes of the fastest process are not well-determined.

The behavior of the rate constants shown in Figure 7 demonstrates why the previous model (Scheme II) was unable to fit the high-temperature data presented here. At 25 °C the forward reaction from lumi to meta I_{380} is sufficiently large compared to the back reaction that the data can be fit with

Table II: Microscopic Rate Constants from Scheme V

k		15 °C	20 °C	25 °C	30 °C	35 °C
k_1	lumi → meta I_{380} (ms^{-1})		0.22 ± 0.07	0.61 ± 0.15	2.4 ± 0.4	4.6 ± 1.1
k_2	meta I_{380} → lumi (ms^{-1})		4.6 ± 4	8.27 ± 3.3	12.4 ± 0.3	16.3 ● 0.6
k_3	meta I_{380} → meta II (ms^{-1})		1.62 ± 0.41	2.50 ± 0.45	3.64 ± 0.4	5.37 ± 0.5
k_4	lumi → meta I_{480} (ms^{-1})	0.34 ± 0.11	0.44 ± 0.07	0.52 ± 0.66	0.93 ± 13	1.38 ± 0.11
k_5	meta I_{480} → meta II (s^{-1})	10.6 ± 0.9	27.3 ± 1.3	67.3 ± 3.7	171 ± 4	327 ± 9
k_6	meta II → meta I_{480} (s^{-1})	12.7 ± 0.8	19.6 ± 0.8	30.8 ± 1.9	52.8 ± 1.6	93.9 ± 2.7

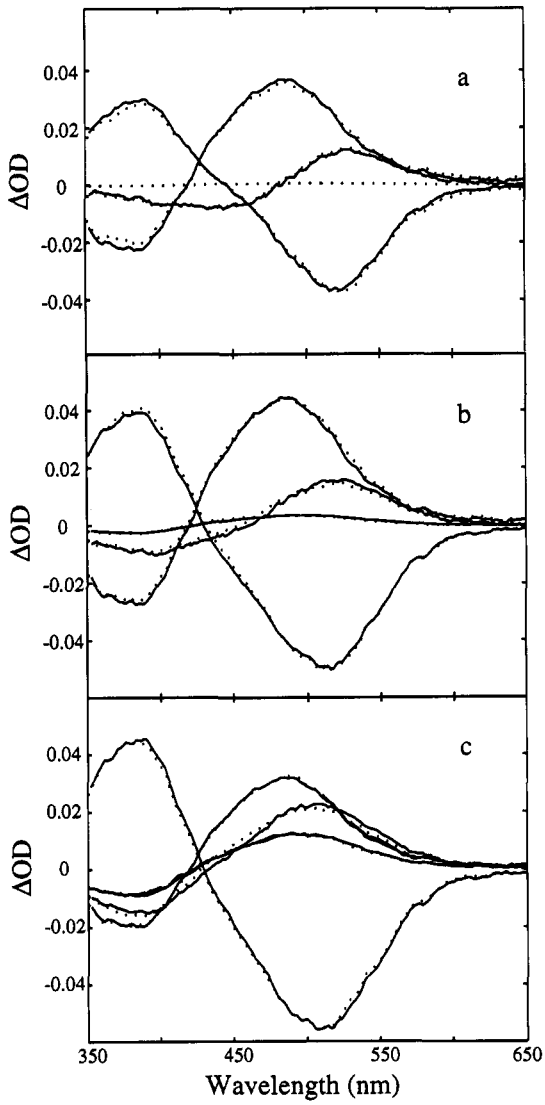

FIGURE 9: Results from the fit to Scheme V. Observed *b* spectra (—) and calculated *b* spectra (···) using the microscopic rate constants are tabulated in Table II and displayed in Figure 8. (a) Results at 15 °C: The microscopic rate constants for k_1, k_2, and k_3 were estimated by extrapolation using values from analysis at the higher temperatures. The amplitude of the first process is small, consistent with the fact that only two exponentials are required to fit the data at 15 °C. (b) Results at 25 °C. (c) Results at 35 °C. The agreement between calculated and observed *b* spectra for 20 and 30 °C was equally good. Eigenvalues for the kinetic matrices gave lifetimes equal to the observed lifetimes to within experimental error for τ_3 and to within 5% for the faster lifetimes (τ_1 and τ_2) where the experimental uncertainty is on the order of 10–20% in most cases.

$k_2 = 0$. Above 25 °C, k_2 becomes large compared to k_1, however, and no reasonable fit can be made if k_2 is neglected. Thus, between 25 and 35 °C a transition occurs from a case in which $(k_3 + k_4)$ determines the fast observed rate to one in which $(k_1 + k_2)$ determines it.

As discussed in the Results section, analyses for this model suffer from multiple local minima in the fitting process, so

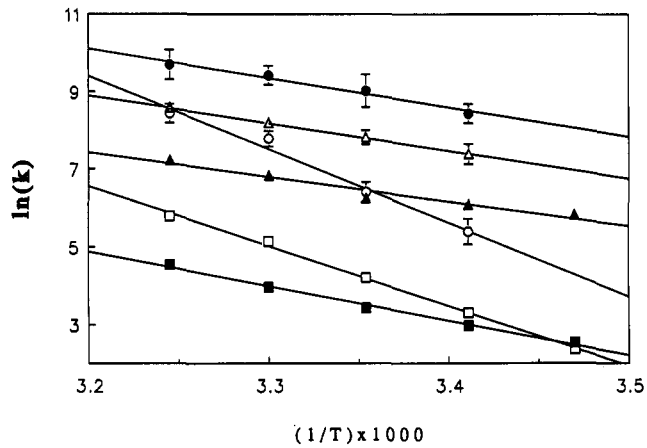

FIGURE 10: Arrhenius plot of microscopic rate constants obtained using Scheme V: (○) k_1; (●) k_2; (△) k_3; (▲) k_4; (□) k_5; (■) k_6. For the numbering of the microscopic rate constants, see the Results section (Scheme V). The activation energies are (kcal) 38.0 (k_1), 15.2 (k_2), 13.1 (k_3), 12.5 (k_4), 30.7 (k_5), and 17.6 (k_6).

Table III: Activation Parameters for Scheme V

	$\Delta H^{\ddagger}$ (kcal/mol)	$\Delta S^{\ddagger}$ (eu)
k_1	37.4 (4)	79.8 (12)
k_2[a]	14.6 (4)	8 (12)
k_3[a]	12.5 (2)	−1 (8)
k_4	11.9 (1.5)	−5.8 (6)
k_5	30.1 (0.5)	50.6 (1.5)
k_6	17.0 (0.5)	5.3 (1.5)
	ΔH (kcal/mol)	ΔS (eu)
K_1[a]	22.5 (9)	71 (20)
K_2	13.1 (0.9)	45.3 (3)

[a] Values are based on data from 20 to 35 °C.

that some uncertainty remains in the exact slopes of the lines of the Arrhenius plot. Still, an interesting qualitative conclusion can be drawn from the plot. Because meta I_{380} intervenes between meta I_{480} and meta II, the extremely large activation energy traditionally associated with the meta I/meta II reaction (Hofmann, 1986) is no longer associated with a single reaction. Instead, this activation energy is divided over two reactions, meta I_{480} → meta I_{380} and meta I_{380} → meta II, each of which has a more normal activation energy.

The Square Model (Scheme V). The microscopic rate constants for Scheme V were obtained separately at each temperature without assuming any functional temperature dependence. Thus, the linearity of the Arrhenius plots for the microscopic rate constants can be taken as support for this scheme. The Arrhenius plot shows that the rate constants associated with the formation of meta I_{380} and meta II have more marked temperature dependences than the remaining four rate constants. The activation parameters, calculated using transition-state theory, reflect this difference (Table III). The formation of these 380 nm absorbing intermediates is associated with both large enthalpies and entropies of activation. Interestingly, the activation parameters for the

lumi → meta I_{480} and the meta I_{380} → meta II are similar, with activation enthalpies near 12 kcal/mol and entropies of activation near zero. This may suggest that the formation of meta II from lumi is essentially a two-step process, and the two pathways of Scheme V differ by the order in which these processes take place. The activation parameters for k_5 and k_6 enable the calculation of the thermodynamic parameters for the final meta I ⇄ meta II equilibrium. The resulting values are 13.1 kcal/mol and 45.3 eu for the enthalpy and entropy, respectively. These values are essentially identical to the ones obtained by Matthews *et al.* (1963).

Comparison of the Mechanisms. Both the equilibrium and square schemes fit our data within experimental error. The residuals obtained with the square model were better than those obtained with the equilibrium model, but this may be a result of the more automated fitting procedure we were able to use for the square model. The presence of multiple local minima when the data were fit to the equilibrium scheme interfered with our attempts to obtain the best fit with that model. The basic problem with the equilibrium scheme is that at high temperatures meta I_{380} is unstable relative to all of the other intermediates and, hence, equilibria are determined as small differences between relatively large microscopic rate constants.

Another factor in favor of the square scheme is the linearity of the Arrhenius plot obtained from it. This was an outcome of the fit for the square model, while for the equilibrium model linearity was one of the criteria imposed during the fitting process. Nevertheless, we believe that deviations from linearity in the Arrhenius plots for either model are within the limits which can be accounted for by experimental uncertainty.

In some ways the pictures presented by both models are similar, i.e., at high temperatures meta I is formed from lumi principally via a precursor containing a deprotonated Schiff's base. The models differ, however, in the significance assigned to meta I_{480}. In the equilibrium case at high temperatures, meta I_{480} is downgraded to a side branch compared to its previous role as a necessary precursor to meta II. In the square model, meta I_{480} becomes the dominant low-temperature path to meta II, but at physiological temperatures it shares its role as the precursor to meta II roughly equally with meta I_{380}. Further work is needed to resolve the true significance of meta I_{480} at physiological temperatures.

Extrapolation, using the activation parameters for Scheme V, yields a predicted lifetime on the order of seconds for lumi at –40 °C. This value appears to be too high, as the lumi → meta I transition temperature is about –40 °C in digitonin extracts (Yoshizawa, 1972). However, treating the formation of meta I_{480} as a simple first-order process, Rapp *et al.* (1970) report a lifetime of 21 s at –40.9 °C in rod disks and suggest that the transition temperature may be elevated in detergent, as they find a decay rate for lumi at –20 °C in digitonin extracts similar to that at –45 °C in rod disks. The environment may affect the stability of lumi and the rate of its decay.

Comparison with Previous Results. The study of absorbance changes following the photolysis of visual pigments by relying on single-wavelength data is hampered by the fact that the photointermediates have overlapping spectra. Thus, there are very few wavelengths at which only one photointermediate contributes to the signal. This problem can sometimes be circumvented by performing measurements at isosbestic points, effectively reducing the number of contributing components. Absorbance changes near 380 nm are mainly due to meta II (and meta I_{380}), but other photointermediates also contribute to the signal at 380 nm, especially meta I_{480}. Previous measurements of the thermal transitions following light excitation in sonicated disk samples on this time scale are single-wavelength measurements, and it is instructive to compare our conclusions to those obtained previously from analyses of kinetics measured at single wavelengths (Lewis *et al.*, 1981; Straume *et al.*, 1990).

The global analysis yields *b* spectra whose relationships to the observed rate constants are analogous to that of the amplitude of an exponential fit to a trace at a single wavelength. These spectra thus provide information in a condensed form and can serve to explain observations that seem puzzling when data from single-wavelength measurements are analyzed. For example, earlier analysis of data from such measurements on retinal rod membrane suspensions seemed to indicate that the lumi/meta I isosbestic point was shifting with temperature from near 490 nm at 10 °C to 440 nm at 36 °C (Lewis *et al.*, 1981). However, the results from Figure 5 suggest another explanation (outlined in the figure caption): The wavelength at which no optical changes are measured is temperature-dependent, but this is not the true isosbestic point between lumi and meta I_{480}. Thus, while the earlier measurements may have contained enough information to reach this conclusion, measurements at individual wavelengths made it difficult to discriminate between the shift of a single band and the growth of a shoulder on a fixed band.

The increase in amplitude of the millisecond component of exponential fits to absorbance changes at 380 nm was explained by Straume *et al.* (1990) as resulting from an increase in the extinction coefficient of meta I at 380 nm, perhaps due to a blue shift in the meta I spectrum. Again, Figure 5 suggests another explanation: A meta II-like intermediate is formed directly from lumi.

The rate constants we observe for the lumi → meta I_{480} reaction are smaller than those typically reported in reviews (10–100 μs near room temperature) (Ostroy, 1977; Shichida, 1986). Comparison between results from the relatively few attempts at measuring meta I formation in ROS at elevated temperatures, by recording transient changes in optical density at single wavelengths, reveals some differences. While some studies have found values near 100 μs (Cone, 1972; Rapp, 1970; Sengbush & Stieve, 1971), other studies have found the rate to be similar to that reported here (Lewis *et al.*, 1981; Straume *et al.*, 1990). Studies that found 100-μs meta I formation may have been detecting the rise of meta I_{380}.

Lamola *et al.* (1974) measured volume changes upon the formation of meta II in both detergent extracts and sonicated ROS. Sonicated ROS preparations gave the largest increase in volume upon the formation of meta II, about 6-fold larger than in the case of digitonin extracts. In harsher detergents, Ammonyx LO and Emulphogene, no increase in volume upon meta II formation was detected. The results were interpreted in terms of the effect of detergents upon the phospholipid environment. The rise in absorbance near 380 nm is greatly accelerated in the "strong" detergents, and in Ammonyx LO detergent it is completed in about 100 μs at 20 °C (Applebury *et al.*, 1974). These changes thus occur on the order of the fastest component observed in this study of sonicated ROS disks. It clearly would be interesting to study the interconversions between the photointermediates in detergent extracts by measuring entire spectra with microsecond time resolution. Perhaps the effect of detergents is similar to that of temperature, such that the formation of meta II occurs mainly through a lumi ⇄ meta I_{380} → meta II path in some detergents, as is the case for disk suspensions at physiological temperatures.

The effects of temperature and pH upon the meta I ⇄ meta II equilibrium have been known since the work of Matthews *et al.* (1963), which showed that meta II is favored by low pH and high temperature. While low pH favors meta II, the role of protons (or OH^-) in the transformations leading to the formation of meta II is simply not clear. The apparent rate constant of meta II formation has been found to decrease with increased pH through a minimum near neutral pH, but to increase with pH under basic conditions (Emrich & Reich, 1974). Parkes and Liebman (1984) found that the actual formation of meta II was base-catalyzed and that the stabilizing effect of lowered pH was due to mass action only. Our preliminary pH studies show that the major effect of pH is on the meta I ⇄ meta II equilibrium constant, consistent with previous conclusions (Parkes & Liebman, 1984). Thus, to a first approximation, only the amplitude of the slowest component is affected and not the observed time constants. This is consistent with a mass action effect of protons. The analysis published here reporting an early 380 nm absorbing intermediate is significant for previous reports of base catalysis of meta II formation since the reduced amplitude of the slow component at high pH could erroneously lead to a conclusion of base catalysis if data are fit with too few exponentials.

Results from laboratories performing site-specific mutagenesis are likely to guide the way in this regard. Glutamic acid 113 has been identified as the primary counterion to the protonated Schiff's base of retinal in rhodopsin (Nathans, 1990; Sakmar *et al.*, 1989; Zhukovsky & Oprian, 1989). Its replacement by a neutral amino acid lowers the p*K* of the protonated Schiff's base of retinal to about 6 and yields a pigment absorbing near 490 nm at low pH and near 380 nm at high pH. The 380-nm form has been shown to contain a deprotonated Schiff's base (Lin *et al.*, 1992). Following regeneration with *all-trans*-retinal, a pigment activating G-protein in the dark is formed, but illumination is required in the case of the 11-*cis* form (Sakmar *et al.*, 1989). It appears that, in the absence of the charge on Glu-113, meta II is formed in the presence of *all-trans*-retinal. Replacement of several histidines has been shown to affect the amount of meta II formed upon illumination. The data suggest that protonation of His-211 stabilizes meta II, while protonation of His-65 and His-152 has the opposite effect (Weitz & Nathans, 1992).

In summary, our results indicate that the rise in absorbance near 380 nm has a fast component in addition to the well-known changes associated with the formation of meta II. Results from spectral analysis do not indicate the presence of a new intermediate *spectrally* distinct from the traditional intermediates (lumi, meta I_{480}, and meta II). Yet, within the framework of first-order kinetics, this kinetic anomaly requires the addition of a new intermediate. By adding such a new intermediate, meta I_{380}, with the spectral characteristics of meta II, we have identified two simple schemes that can account for the observations. Within our temporal and spectral resolution, we find no compelling evidence for differences in the meta I_{380} and meta II spectra, but small differences may exist and perhaps be amplified by changes in the lipid environment or upon substitution of protein residues by site-directed mutagenesis. Varo and Lanyi (1990) suggested the existence of two spectrally identical M-intermediates during the photocycle of bacteriorhodopsin on the basis of a kinetic argument, and it was only later that spectral differences were observed in studies of the photocycle of site-directed mutant bacteriorhodopsins (Thorgeirsson *et al.*, 1991; Varo & Lanyi, 1991; Varo *et al.*, 1992).

Above room temperature, the formation of metarhodopsin II is achieved without a large transient accumulation of metarhodopsin I. The time evolution of the spetra is inconsistent with the traditional scheme: lumi → meta I_{480} ⇄ meta II. Within the framework of first-order kinetics, these observations can be explained by either of two simple kinetic schemes that lead to the formation of meta II directly from lumi without the formation of meta I_{480}. Both schemes contain a new intermediate, meta I_{380}, which is spectrally similar to meta II but is formed from lumi in less than 100 μs. The two schemes provide somewhat different explanations for the observed early rise in absorbance near 380 nm, as one scheme postulates that the later photointermediates are connected by strongly coupled equilibria while the other scheme contains a branched step for lumi decay.

APPENDIX

Several first-order schemes considered in this study are listed here, along with a brief explanation of how they fit the data.

Schemes Inconsistent with the Results. Schemes A and B can be eliminated as they predict that only two apparent rates would be measured. Furthermore, it was not possible to obtain temperature-invariant spectra using results from two-exponential fits. Schemes C and D cannot account for the changes in the shape of the *b* spectrum associated with the second apparent rate, and scheme D is inconsistent with a temperature-invariant spectrum at 1 μs following photolysis. Schemes E and F were previously suggested (Thorgeirsson *et al.*, 1992) on the basis of results obtained at 25 °C and provided an adequate explanation of results at temperatures between 15 and 30 °C (Thorgeirsson, 1992). These schemes are now excluded on the basis of their inability to account for the large amplitude of the fastest component at 35 °C.

Schemes Consistent with the Results. Schemes G–L can account for the results. Schemes G and I were rigorously tested, while schemes H and J–L are modifications of schemes G and I in a way that would not lead to differences testable by our methods. Schemes G and I are thus preferred as they are the simplest schemes found to account for all of our data.

The small increase in the value of k_3 observed with scheme G at lower temperatures (see Results section) can be removed by adding another microscopic rate constant. Take, for example, the modification shown in scheme H. A separate path to meta I from lumi removes the need for large values of k_3 at low temperature, as the formation of meta I_{480} is not inhibited when the lumi ⇄ meta I_{380} equilibrium favors lumi. This scheme, however, is very similar to, but more complicated than, scheme I.

The data presented here are not consistent with the complete formation of meta I from lumi on a time scale of tens of microseconds near room temperature. We cannot exclude the attainment of an equilibrium on a microsecond time scale between lumi and a meta I_{480} intermediate if the equilibrium favors the lumi intermediate. To account for the slower formation of meta I_{480} (i.e., 2.8 ms at 15 °C), however, either a time-dependent equilibrium constant would have to be postulated or another meta I_{480} intermediate added to the scheme. For example, a kinetic scheme like scheme J is a possibility. A rapid equilibrium is established between lumi, meta I_{480}, and meta I_{380}, followed by a slower change yielding another spectrally similar set of intermediates, perhaps in a different protein conformation. Nothing in our data justifies postulating this more complicated scheme, but increased complexity might facilitate the task of explaining the effects

Scheme VI

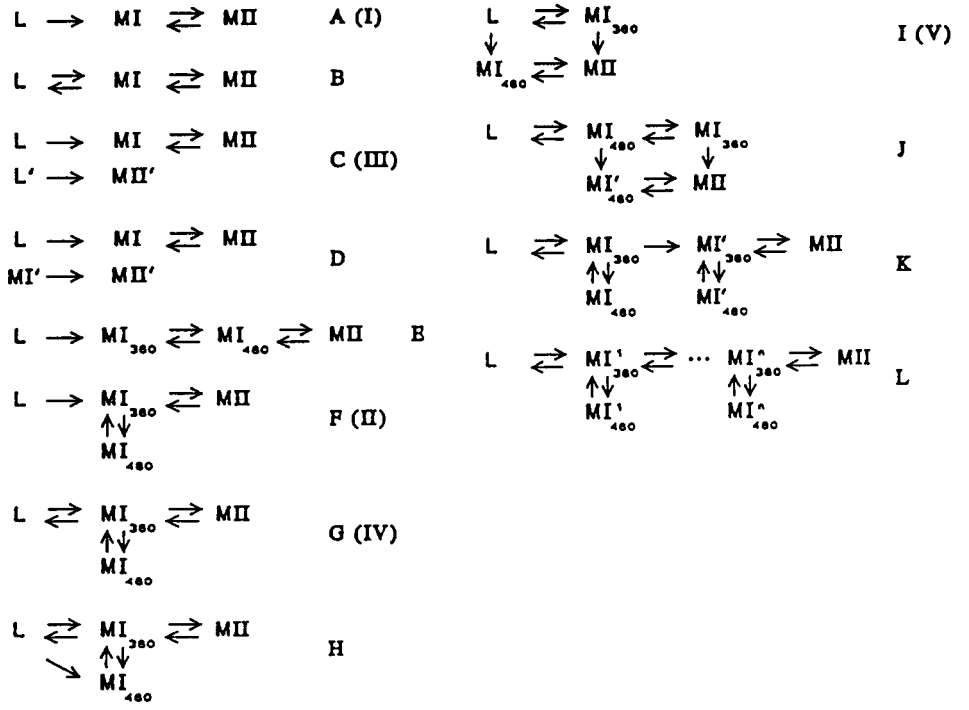

of temperature and lipid environment on the kinetics of the transitions following lumi formation. The first equilibrium could, for example, yield a very small transient rise (at wavelengths to the blue of 480 nm) between 10 and 100 μs following excitation that perhaps could be measured with adequate signal-to-noise in a single-wavelength measurement. Two different meta I_{480} intermediates could account for the difference between the activation parameters measured at high and low temperatures for the lumi → meta I_{480} reaction and perhaps the "second-order character" during the initial stages of meta I formation (Rapp, 1970; Rapp *et al.*, 1979). Williams and co-workers have suggested that there is more than one isospectral form of the meta I intermediate (Stewart *et al.*, 1977).

In a similar vein, scheme K would fit the data. This scheme bears some resemblance to a scheme recently proposed for the photocycle of bacteriorhodopsin (Lanyi, 1992). A key transition in the photocycle of bacteriorhodopsin is the formation of the M-intermediate which, like meta II, contains a deprotonated Schiff's base of retinal. Many explanations have been invoked to explain the multiphasic M-rise kinetics involving two or more spectrally indistinguishable M-intermediates (Kouyama *et al.*, 1988; Dancshazy *et al.*, 1988; Bitting *et al.*, 1990; Ames & Mathies, 1990). A recent model is that of Varo and Lanyi who, after analyzing photocycle data under a variety of conditions, suggested two intermediates separated by a largely irreversible protein conformation change (Varo & Lanyi, 1991; Lanyi, 1992). Rhodopsin and bacteriorhodopsin have different functions, but deprotonation of the chromophore appears to be a key event both in proton translocation by bacteriorhodopsin (Longstaff & Rando, 1987) and in the activation of G-protein by the meta II form of rhodopsin (Longstaff *et al.*, 1986). It is unlikely that the formation of meta II is a single concerted reaction as it involves at least three events: deprotonation of the chromophore, a large conformational change, and proton uptake. During the bacteriorhodopsin photocycle the M-intermediate is formed in less than 100 μs, and it is conceivable that in rhodopsin, too, the event triggering the conformational change involves an equally fast protonation–deprotonation reaction at the chromophore.

Schemes A–K are discrete first-order approximations to processes that may, in fact, involve multiple spectrally similar intermediates. The absorbance measurements are only sensitive to the immediate environment of the chromophore, and processes may be going on that have little or no signature in the absorbance spectrum. While our results are consistent with the formation of two species with the spectral characteristics of meta II, other types of kinetic schemes involving a large number of spectrally similar intermediates, such as scheme L, have by no means been ruled out. Protein dynamics may not be adequately described by simple kinetic schemes involving a few discrete intermediates, and analysis in terms of a power law or a stretched exponential (Ansari *et al.*, 1985; Dewey & Spencer, 1991; Liebovitch *et al.*, 1987; Nagle, 1993; Oswald *et al.*, 1991) might yield interesting insights.

REFERENCES

Albeck, A., Friedman, N., Ottolenghi, M., Sheves, M., Einterz, C. M., Hug, S. J., Lewis, J. W., & Kliger, D. S. (1989) *Biophys. J. 55*, 233–241.

Ames, J. B., & Mathies, R. A. (1990) *Biochemistry 29*, 7181–7190.

Ansari, A., Berendzen, J., Browne, S. F., Frauenfelder, H., Iben, I. E., Sauke, T. B., Shyamsunder, E., & Young, R. D. (1985) *Proc. Natl. Acad. Sci. U.S.A. 82*, 5000–5004.

Applebury, M. L., Zuckerman, D. M., Lamola, A. A., & Jovin, T. M. (1974) *Biochemistry 13*, 3448–3458.

Bitting, H. C., Jr., Jang, D.-J., El-Sayed, M. A. (1990) *Photochem. Photobiol. 51*, 593–598.

Cone, R. A. (1972) *Nature New Biol. 236*, 39–43.

Dancshazy, Z., Govindjee, R., Ebrey, T. G. (1988) *Proc. Natl. Acad. Sci. U.S.A. 85*, 6358–6361.

Dewey, T. G., & Spencer, D. B. (1991) *Comments Mol. Cell. Biophys. 7*, 155–171.

Emrich, H. M., & Reich, R. (1974) *Z. Naturforsch. 29c*, 577–591.

Henry, E. R., & Hofrichter, J. (1992) *Methods Enzymol. 210*, 129–193.

Hofmann, K. P. (1986) *Photobiochem. Photobiophys. 13*, 309–327.
Hug, S. J., Lewis, J. W., Einterz, C. M., Thorgeirsson, T. E., & Kliger, D. S. (1990) *Biochemistry 29*, 1475–1485.
Kouyama, T., Nasuda-Kouyama, A., Ikegami, A., Matthew, M. K., & Stoeckenius, W. (1988) *Biochemistry 27*, 5855–5863.
Lamola, A. A., Yamane, T., & Zipp, A. (1974) *Biochemistry 13*, 738–745.
Lanyi, J. K. (1992) *J. Bioenerg. Biomembr. 24*, 169–179.
Lewis, J. W., & Kliger, D. S. (1992) *J. Bioenerg. Biomembr. 24*, 201–210.
Lewis, J. W., Winterle, J. S., Powers, M. A., Kliger, D. S., & Dratz, E. A. (1981) *Photochem. Photobiol. 34*, 371–384.
Lewis, J. W., Warner, J., Einterz, C. M., & Kliger, D. S. (1987a) *Rev. Sci. Instrum. 58*, 945–949.
Lewis, J. W., Hug, S. J., & Kliger, D. S. (1987b) *Rev. Sci. Instrum. 58*, 2342–2345.
Liebovitch, L. S., Fischbarg, S. J., & Koniarek, J. P. (1987) *Math. Biosci. 84*, 37–68.
Lin, S. W., Sakmar, T. P., Franke, R. R., Khorana, H. G., & Mathies, R. A. (1992) *Biochemistry 31*, 5105–5111.
Longstaff, C., & Rando, R. R. (1987) *Biochemistry 26*, 6107–6113.
Longstaff, C, Calhoon, R. D., & Rando, R. R. (1986) *Proc. Natl. Acad. Sci. U.S.A. 83*, 4209–4213.
Matthews, R. G., Hubbard, R., Brown, P. K., & Wald, G. (1963) *J. Gen. Physiol. 47*, 215–240.
Millhauser, G. L., & Oswald, R. E. (1988) *Synapse (N.Y.) 2*, 97–103.
Nagle, J. F. (1993) *Biophys. J. 63*, 366–370.
Nagle, J. F., Parodi, L. A., & Lozier, R. H. (1982) *Biophys. J. 38*, 161–174.
Nathans, J. (1990) *Biochemistry 29*, 9746–9752.
Ostroy, S. E. (1977) *Biochim. Biophys. Acta 463*, 91–125.
Oswald, R. E., Millhauser, G. L., & Carter, A. A. (1991) *Biophys. J. 59*, 1136–1142.
Parkes, J. H., & Liebman, P. A. (1984) *Biochemistry 23*, 5054–5061.
Rapp, J. (1979) *Vision Res. 19*, 137–141.
Rapp, J., Wiesenfeld, J. R., & Abrahamson, E. W. (1970) *Biochim. Biophys. Acta 201*, 119–130.
Sakmar, T. P., Franke, R. R., & Khorana, H. G. (1989) *Proc. Natl. Acad. Sci. U.S.A. 86*, 8309–8313.
Schoenlein, R. W., Peteanu, L. A., Mathies, R. A., & Shank, C. V. (1991) *Science 254*, 412–415.
Sengbush, G. v., & Stieve, H. (1971) *Z. Naturforsch. 26b*, 488–489.
Shichida, Y. (1986) *Photobiochem. Photobiophys. 13*, 287–307.
Stewart, J. G., Baker, B. N., & Williams, T. P. (1977) *Biophys. Struct. Mech. 3*, 19–29.
Straume, M., Mitchell, D. C., Miller, J. L., & Litman, B. J. (1990) *Biochemistry 29*, 9135–9142.
Stryer, L. (1986) *Annu. Rev. Neurosci. 9*, 87–119.
Thorgeirsson, T. E. (1992) *Ph.*D. Thesis, University of California at Santa Cruz, Santa Cruz, CA.
Thorgeirsson, T. E., Milder, S. J., Miercke, L. J. W., Betlach, M. C., Shand, R. F., Stroud, R. M., & Kliger, D. S. (1991) *Biochemistry 30*, 9133–9142.
Thorgeirsson, T. E., Lewis, J. W., Wallace-Williams, S. E., & Kliger, D. S. (1992) *Photochem. Photobiol. 56*, 1135–1144.
Varo, G., & Lanyi, J. K. (1990) *Biochemistry 29*, 2241–2250.
Varo, G., & Lanyi, J. K. (1991) *Biochemistry 30*, 5008–5015.
Varo, G., Zimanyi, L., Chang, M., Ni, B., Needleman, R., & Lanyi, J. K. (1992) *Biophys. J. 61*, 820–826.
Weitz, C. J., & Nathans, J. (1992) *Neuron 8*, 465–472.
Yoshizawa, T. (1972) in *Handbook of Sensory Physiology vol. Vii/1* (Dartnall, H. J. A., Ed.) pp 145–179, Springer-Verlag, Berlin.
Zhukovsky, R. S., & Oprian, D. D. (1989) *Science 246*, 928.